Dynamics of Infinite and Finite Bubbles Induced by Geometrical Constraint

Zuonaki Ongodiebi and Adokiye Omoghoyan

Abstract: We present an experimental study and characterise the dynamics of the propagation modes that occur due to the displacement of a viscous fluid by finite and infinite bubbles from microchannels with centered rectangular occlusions. The centered rectangular occlusion results in a family of steadily propagating fingers/bubbles analogous to the propagation modes observed in millimeter scale tubes, indicating that gravity is not an essential physical mechanism that underpins the emergence of these states. We found that the transition from symmetric to either localized or oscillatory state results from exchange of stability between two different states rather than a continuous evolution from one state to another. Also, our experimental evidence revealed that infinite (air finger) and finite bubbles of aspect ratios $\alpha > 1$ (defined as $\alpha = L/W$ where L is the distance between the front and the rear of the bubble measured in its static symmetric state and W is the width of the bubble) exhibit propagation modes that are both quantitatively and qualitatively similar; but short bubbles with $\alpha < 1$ undergo a transition similar to that of a continuous transition from one state to another.

Keywords: bifurcation, bubbles, Evolution, Microfluidics, Stability, Transition, Two-phase flow.

1 Introduction

Understanding the flow of confined bubbles and droplets within natural and man-made channels reveal a wide range of industrial applications ranging from enhanced oil recovery to microfluidic chip-based chemical analysis. Microfluidics; which refers to a set of technologies used for controling the flow dynamics of very small amount of liquid and gases in a miniaturised system is an emerging research area not only due to reduced sample volumes and cost involved when compared with macro-sized components, but the ability to easily and accurately control the dynamics of the flow. In these systems, there is competition between in-

terfacial, viscous and/or capillary forces. The study of viscous oil-water flows [25] and complex fluid flow [26] in microchannel at low Reynolds number are examples of viscous forces dominated flows while an experimental investigation of capillary instabilities in a microfluidic T-Junction by [27] analogous to the classical Plateau-Rayleigh instabilities is dominated by interfacial forces. Liquid-gas and liquid- liquid flows in microchannels have received increasing experimental research interests [1], [2]. Bubbly flow in microchannel have been shown to be very effective in heat transfer [5] and can effectively transport reagents and encapsulate cells to perform chemical reactions and biological experiments with high sensitivity [3], [4]. The ink-jet printing (a type of computer printing that creates a digital image by propelling droplets of ink onto paper, plastic or other substrates) is a product of an understanding of bubbles/droplets dynamics in con- fined geometries. Advances in digital microfluidics (an alternative technology for microfluidic systems based upon design, composition and manipulation of discrete droplets and bubbles) have facilitated the understanding of diverse and complex flow dynamics in microchannel network, as the formation, transport and merging of bubbles/droplets in microchannels are well understood [20]. Bubbles/droplets traveling through microchannel had been successfully applied to encode and decode information and perform logical operations [21], [22]. The displacement of one fluid by another immiscible fluid of lower viscosity (usually air) through a channel at fixed flow rate, results to the formation of long bubble (air finger) which significantly interacts with the channel geometry. This two-phase displacement flow is a fundamental fluid mechanics phenomenon such as the flow of oil and gas in oil pipelines, extraction of oil from porous media [6], mammalian breathing, biomechanics of the lungs [7], pulmonary airways [8] and emerging lab-on-chip technologies [12]. Many of such two-phase displacement studies have been performed in simple geometries such as rectangular and elliptical [9], polygonal [10] and circular cross-sections [11]. In these geometries, a family of steadily propagating air fingers is formed when air is introduced at a constant flow rate. These fingers are centered within the tube and are surrounded by a film of the viscous liquid. The film deposited at the walls of the capillary, which increases monotonically with the capillary number $Ca = \frac{\mu U}{\sigma}$ (which is the ratio of viscous to surface tension forces where μ is the fluid viscosity, U is the velocity of the bubble and σ, the surface tension), causes the bubble to move faster than the average speed of the fluid

[12]. Further studies of the mechanics of pulmonary airway reopening was experimentally investigated by driving an air finger through a collapsed fluid filled elastic tube [23]. In most practical applications however, more complex geometries are involved. For example, the pores in carbonate oil reservoirs are irregular and consists of sudden changes in pore shapes and sizes [13] and airway collapse or mucus build-up in the lungs [14].

Recently, [15], [16] introduced a centred partial occlusion in millimetric tubes of rectangular cross-section and uncovered multiple finger propagation modes when air is driven through a channel filled with viscous fluid. Similar study by [17] revealed that for sufficiently high occlusions, two alternative stable solutions are possible for low flow rates: a steadily propagating asymmetric air finger that spans the majority of the tube or a steadily propagating asymmetric air finger that localized within one of the side-channels. A two-dimensional numerical investigation of finger propagation modes captured all the finger dynamics earlier reported, and in addition, revealed a new mode of finger behaviour such as bifurcation associated with tip-splitting [18]. These recent findings of [15], [16], [17], [18] have shown that a change in pore geometry alters the dynamics of an air finger/bubble, indicating that models based on idealized pore geometries are not able to capture key features of complex practical flows, whose understanding is the motivation behind the present study. In this study, we experimentally investigated and confirmed that the multiplicity of propagation modes uncovered in millimetric channels also exist in microchannels indicating that gravitational force does not dictate the physical mechanism that underpins the emergence of the multiple propagation modes.

2 Experimental Methods

A schematic diagram of the experimental setup is shown in figure 1. The experiments were performed in three microchannels; labelled Channels 1, 2 and 3. The channels have constant height and length of 300 ± 5 μm and 9.60 ± 0.05 cm respectively with a rectangular centered partial occlusion each having constant length of 9.0±0.05 cm thereby leaving a length of 0.60 ± 0.05 cm unoccluded space in all three channels to allow initial states of the fingers/bubbles to be symmetric before driving them through the occluded part of the channels. The widths of both the channels and the obstacles were measured with a travelling micro-

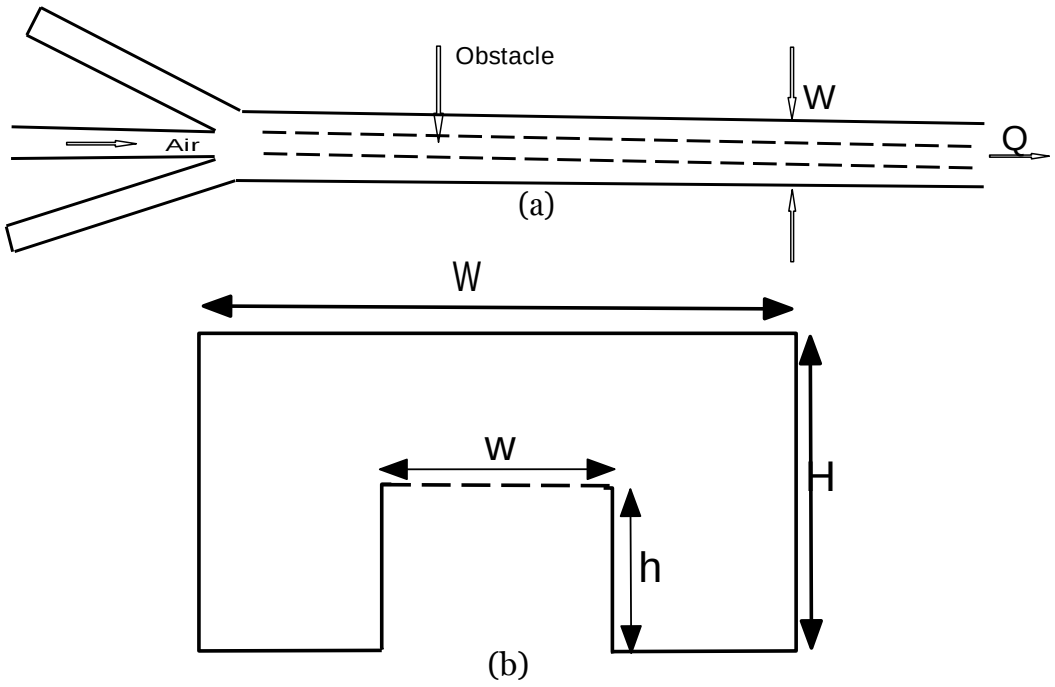

Figure 1: Schematic diagram of the experimental setup and microchannel cross- sectional geometry. Three channels were used for the experiment. Figure 1 (a) illustrates how liquid is withdrawn at constant flow rate Q from one end of the initially liquid-filled tube, with two of the outlets at the other end of the channel occluded for the production of an Infinite (long) bubble while no outlet is occluded for the production of finite (short) bubble. Figure 1 (b) is the cross section of the channel. The outer width and height of the cross section are W and H respectively, while the corresponding centered rectangular occluded cross section are w and h respectively. See table 1 for detailed cross-sectional dimensions.

scope. The measurements were done at five regularly spaced locations along each channel and obstacle from which averaged values were determined and shown in table 1. Each tube has three outlets at the beginning and an outlet at the rear. See figures 1 (a & b) for top and side views of the channel. The channels were manufactured by micro-milling of a piece of perspex (CAT3D-M6, CNC, milling machine, Datron Technologies Ltd), and sealed with a clear adhesive film (Corning), which was supported by a precision- milled flat perspex lid. Each channel was completely filled with Galden HT 270 (Perfluorinated fluid from Solvay Solexis of density ρ = 1856 kg/m^3, with dynamic viscosity μ = 0.0313 Pa.s both measured in our controlled laboratory temperature at 21 ± 1^oC and surface tension value of 0.02 N/m specified by the manufacturer) for the experiment. Infinite (long) bubbles were produced by driving in air at a constant volume flux Q imposed by

withdrawing the liquid at the end of the tube with two of the three outlets closed and completely filled with viscous liquid. These flow rates were produced with a syringe pump (KDS 210 KD scientific) connected to 500 μl syringe attached to the end of the channel through a flexible tubing. Finite bubbles were formed at the beginning of the unoccluded part of the channels with the three outlets open to the atmosphere, by manually injecting air into the tube with a low constant flux flow. The air was injected with a 500 μl syringe and needle. We were able to produce different sizes of finite bubbles of unknown volumes, which we characterized by measuring their static symmetric length L (defined as the distance between the front and rear of the bubble). A short unoccluded rectangular inlet section ensured that the bubble was initially symmetric about the mid-plane of the tube. The motion of the steadily propagating finger/bubble tips were recorded at the rate of 100 frames per second with high speed (PCO) still camera with resolution (1280 × 1024) mounted on a 60 mm lens placed at a distance of 8.8 ± 0.05 cm above the microchannel. A LED light was difused through a sheet of tracing paper placed under the channel to capture the dynamics of the fingers/bubbles for different flow rates Q. The velocity of the finger/bubble tip position U, between frames, and hence the capillary number Ca, which is a measure of the propagation speed were determined from image analysis of the frames with MATLAB. The aspect ratio of the channel; $\alpha = W/H$ (ratio of the width W and height H of the channel) lies in the range $1 \leq \alpha \leq 10$ typical of microfluidic channels [10].

Table 1: Channel and Obstacle dimensions. W and H denote the width and height of the channel while w and h represent the respective width and height of the obstacle.

Channels	$W \pm 5\,\mu$m	$H \pm 5\,\mu$m	$w \pm 5\,\mu$m	$h \pm 5\,\mu$m
Channel 1	1000.4	300	350.2	150
Channel 2	900.2	300	332	100
Channel 3	1000	300	333.4	150

3 Results

Infinite Bubbles/Air Fingers.

The morphology of an infinite bubble as it propagates through the tube depends strongly on Ca and the obstacle dimension. In our experimental measurements, this is observed by the changes in the shape of the bubbles and also, in the measurements of the bubble velocity. The nature of these bubbles and their oil re-

covery properties is a function of a bulk measure of the fluid displacement given by the wet fraction $m = 1 - Q/AU$, where Q is the flow rate, U is the velocity of the bubble and $A = WH - wh$ is the cross-sectional area of the tube. We adopt the same measure to characterise the motion of finite bubbles but in the case, we are unable to provide a physical interpretation for m. Top-views of the different types of fingers or infinite bubbles observed in our experiments are shown in figures (2 - 5). The arrows indicate the direction of motion of the finger/bubble.

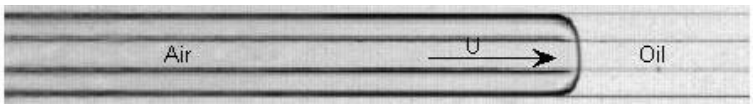

Figure 2: Symmetric finger; the arrow indicates the direction of flow in all cases. $Ca = 0.0026$ Channel 2

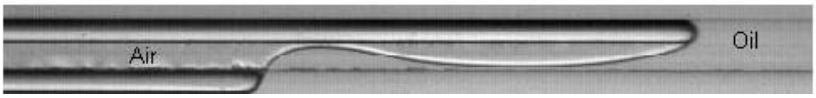

Figure 3: Asymmetric finger. $Ca = 0.014$ Channel 1

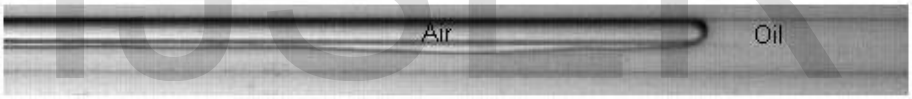

Figure 4: Localized finger. $Ca = 0.032$ Channel 3

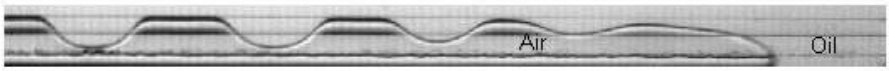

Figure 5: Oscillatory finger. $Ca = 0.057$ Channel 2

Bifurcation graphs

We conducted several series of experiments in the three tubes initially filled with viscous fluid and driving in air through the tubes by withdrawing the liquid at the end of each tube. The flow rate was incremented in steps of $Q = 30$ μl/min. At low values of capillary number, a thin film of fluid was deposited on the tube wall behind the advancing bubble tip. As Ca is increased, which

corresponds to increasing Q, a thicker film of fluid is deposited on the walls of the tubes. This is because the interface curvature increases due to increase in fluid pressure that drives the axial flow. Further increment of Ca above a critical capillary number Ca_C, the symmetric bubbles lose stability to asymmetric non-localized bubbles which subsequently, localized through symmetry-breaking [19]. The localized finger selects a path of least constricted region of the tube cross-section. This is because, the minimal but unavoidable imperfection in the manufacturing of the obstacle, introduced bias into the system. Figure 6 is a plot of a bifurcation graph of channel 1 obtained by constant increment of the flow rate in steps of Q = 30 μl/min. The experiment was conducted at the beginning and at the end of the channel. Each data point represents a single experiment. At low capillary number, $0 < Ca \leq 0.012$, sym- metric fingers propagate through the tube both at the beginning and at the end. As the capillary number increases not beyond Ca_C = 0.012, there is a monotonic increase in the wet fraction. Further increment of the capillary number beyond Ca_C deforms the tip of the advancing finger due to increased in fluid pressure, a feature common to many front propagating systems such as bubbles advancing in rigid tubes and Hele-Shaw channels [9], [11], [16], [17], [24]. The increase in the fluid pressure, causes the finger to lose its symmetry about the vertical midplane running parallel to the length of the tube, thereby selecting a path of least resistance and localizes at one side of the channel wall shown in the inset of figure 6. Similar scenario as in channel 1 was also ob- served in channel 3 as shown in figure 7. In channel 2 with lower obstacle height, we observed symmetric fingers at lower capillary numbers. As the capillary number exceeds the critical capillary value of Ca_C = 0.032, the axial symmetry of the finger is broken, which almost smoothly transcends to asymmetric non-localized finger in which the tip propagates with an almost constant shape and speed, but leaves behind a spatially varying periodic disturbance. Top-view images of a symmetric and oscillatory fingers are shown in the inset of figure 8. This unique but complex finger propagation mode is described by [19] to have manifested due to the existence of a symmetry-breaking pitchfork bifurcation between the symmetric and asymmetric steady states while [15] suggested that a global homoclinic connection gave rise to the oscillatory propagation modes.

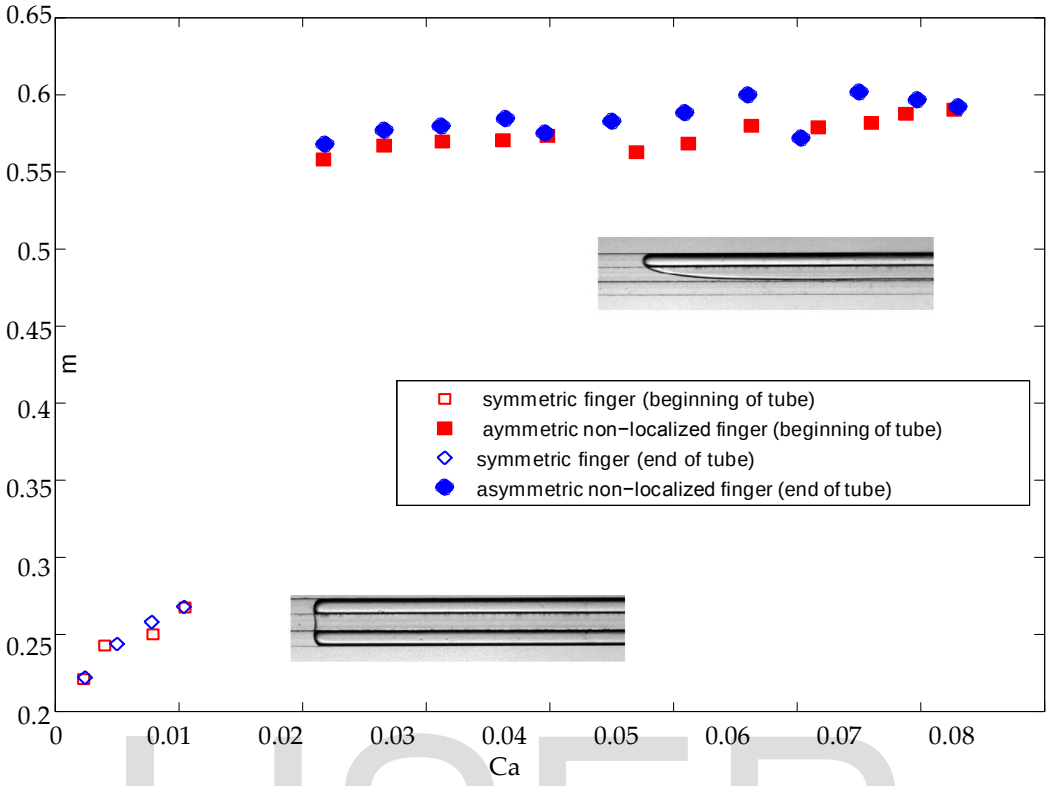

Figure 6: Channel 1: Wet fraction m as a function of capillary number Ca. The insets are top-view images of air fingers propagating through the channel from right to left. Each data point represents a single experiment. The experiment was conducted at the beginning and at the end of the channel.

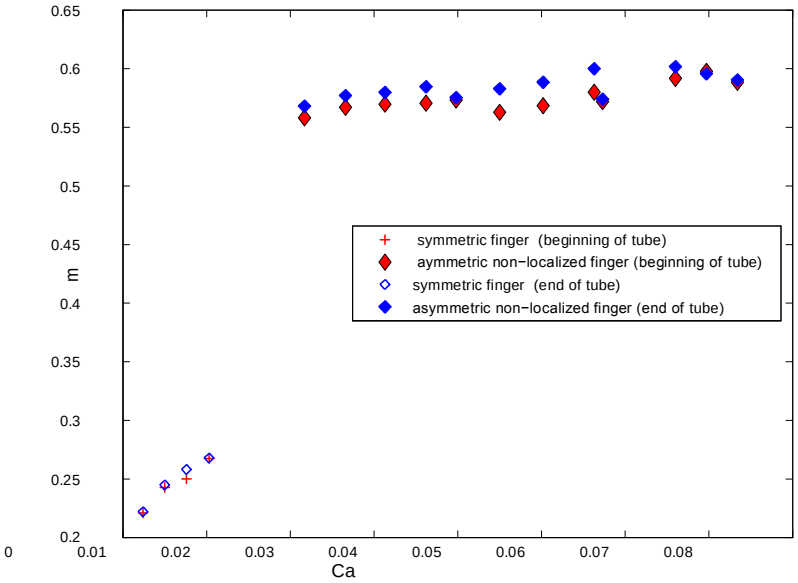

Figure 7: Channel 3: Wet fraction m as a function of capillary number Ca. Each data point represents a single experiment. The experiment was conducted at the beginning and at the end of the channel

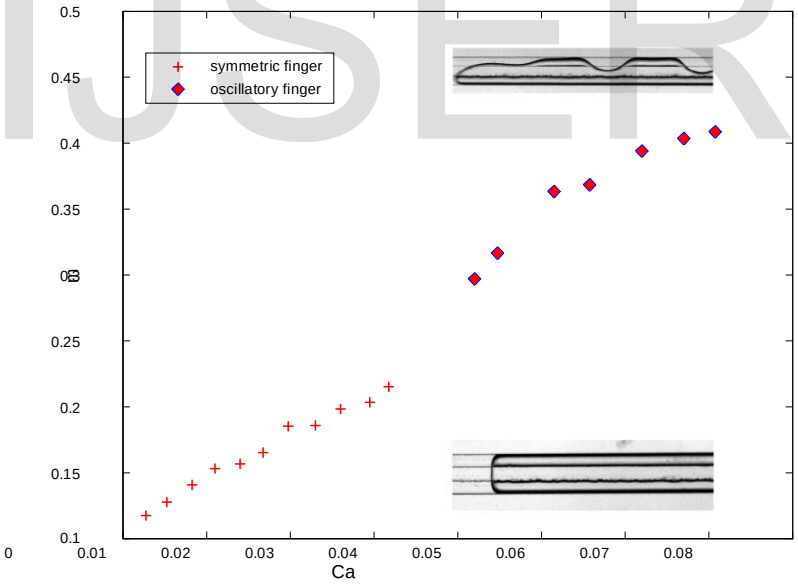

Figure 8: Channel 2: Wet fraction m as a function of capillary number Ca. The insets are top-view images of air fingers propagating through the channel from right to left. Each data point represents a single experiment conducted at the end of the channel

Finite Bubbles

We conducted the experiment with bubbles of different aspect ratios (defined as $\alpha = L/W$ where L is the distance between the front and the rear of the bubble measured in their static symmetric states and W is the width of the bubble) and make comparism of the data obtain for finite bubbles with infinite bubbles under the same experimental condition. Each bubble was driven through the fluid filled channel by withdrawing the fluid at the end of the channel with constant increment of Q = 30 μl/min. Figures (9-12) are top-view images of finite bubbles exhibiting different propagation modes. In fig. 13, we present the responses of finite bubbles of different aspect ratios (α) when subjected to the same flow rate. We plotted the global measure m as a function of Ca in all cases. Bubbles with $\alpha > 1$ increases monotonically and almost perfectly aligned with increase in Ca in their symmetric states and also exhibit similar pattern when in their localized states. But there is significant deviation of the data points for the bubble with $\alpha = 1$; for reasons we are not able to conclude at this point, but we believe there was an additional inherent drag force due to the balance between the length (L) and width (W) of the bubble. The propagation speeds of finite bubbles are generally less than that of infinite bubbles for the same flow rate due to the presence of a rear meniscus inducing additional drag as noted by [16] who also reported that bubbles too small to be deformed by the tube geometry, will simply act as passive tracers that will follow the flow streamlines thereby, creating a qualitative change in the flow dynamics. The inset in figure 13 is a finite bubble of α = 7/5 when in symmetric and localized states.

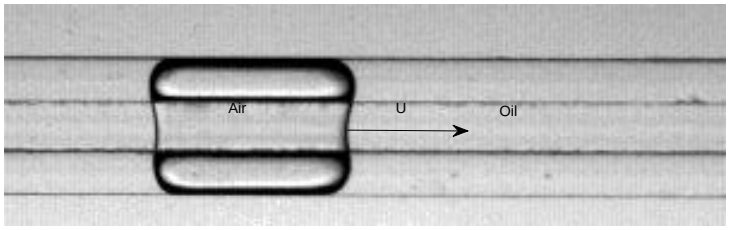

Figure 9: Symmetric finite bubble; the arrow indicates the direction of flow in all cases. Ca = 0.0025 Channel 3

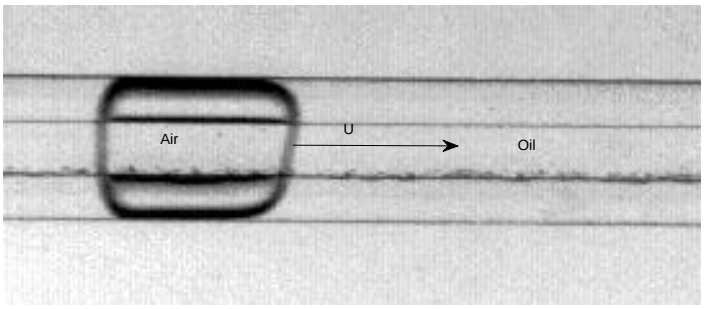

Figure 10: Asymmetric finite bubble. Ca = 0.013 Channel1

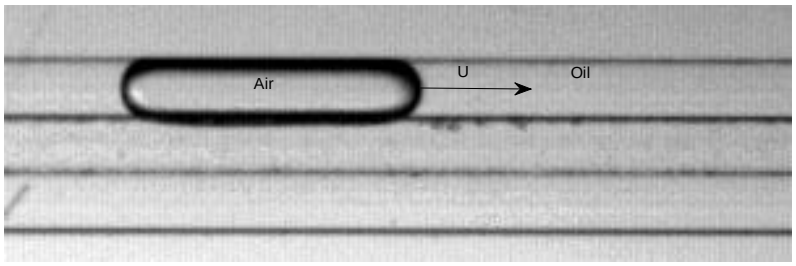

Figure 11: Localized finite bubble. Ca = 0.047 Channel 3

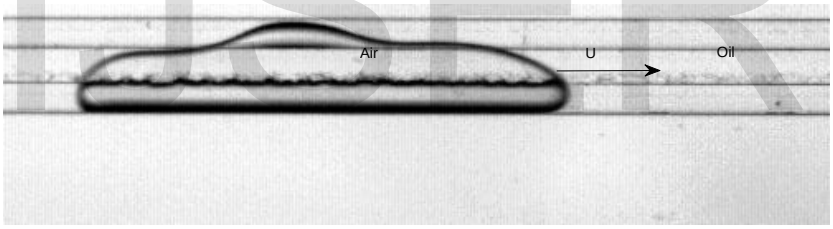

Figure 12: Oscillatory finite bubble. Ca = 0.053 Channel 2

The series of top-view pictures as above, clearly revealed that infinite and finite bubbles exhibit similar propagation states. Similar experiments were also conducted in channel 2 with bubbles of α = 1.3 and α = 0.97 and plotted on the same graph with an infinite (air finger) bubble shown in figure 14. While the air finger and the finite bubble with α = 1.3 revealed obvious bifurcation point, finite bubble with α = 0.97 undergo an almost continuous transition from one state to another.

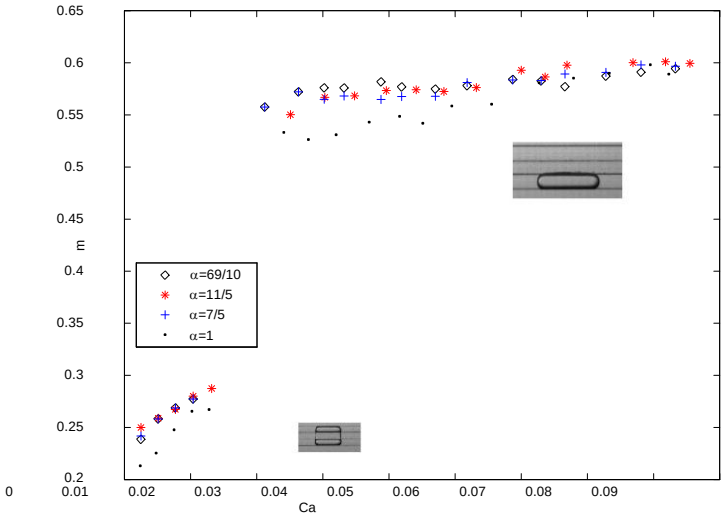

Figure 13: Channel 3: Wet fraction m as a function of capillary number Ca. We considered four bubbles with different aspect ratios as shown above. The aspect ratios are characterized as the ratio of the length and width of the bubbles measured in their symmetric static states. The insets are top-view images of a bubble with α = 7/5 in symmetric and localized states propagating through the channel from right to left. Each data point represents a single experiment.

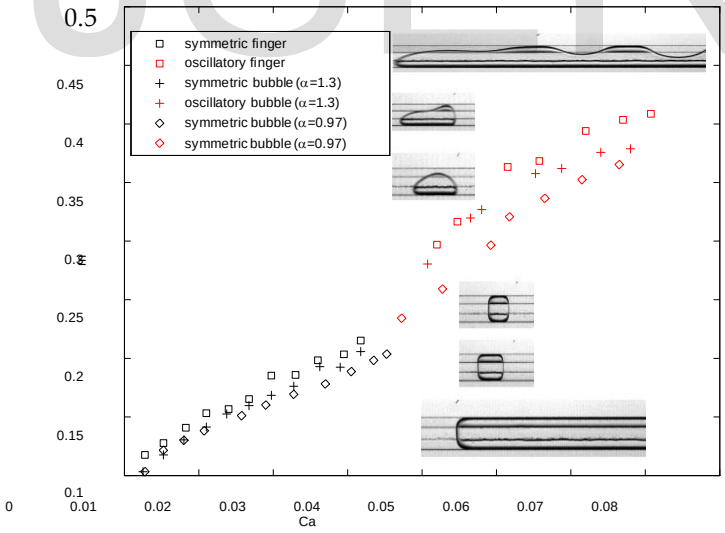

Figure 14: Channel 2: Wet fraction m as a function of capillary number Ca. The insets are top-view images of an air finger and two finite bubbles in their symmetric and oscillatory states as they propagate through the channel from left to right. Each data point represents a single experiment.

4 Conclusions

The results of an experimental investigation of the propagation of air finger/bubble through a fluid-filled rectangular microchannel tubes with centered rectangular partial occlusion have been presented. A simple modification of the tube geometry is evident to have fundamentally ultered the dynamics of bubble propagation induced by constant flux. In addition to the single, symmetric mode seen in unoccluded channels, there exists asymmetric, localized and oscillatory modes in our occluded microchannels analogous to the family of propagating fingers recently uncovered by [16], [15] in millimetre-scale tubes, indicating that gravity is not an essential physical mechanism that underpins the emergence of these states. Our results have shown that infinite and finite bubble ($\alpha > 1$) exhibits propagation modes that are quantitatively and qualitatively similar. We observed symmetric finger/bubble at low capillary numbers which lost symmetry to either asymmetric, localized or oscillatory fingers/bubbles through supercritical symmetry-breaking bifurcation as the capillary number increases beyond a given threshold. Our results revealed almost continous transition between states for a short bubble with characteristic aspect ratio less than one. Symmetric fingers are noted for greater oil recovery property while the asymmetric, localized and oscillatory fingers limit the amount of liquid recovered.

The support of PTDF is gratefully acknowledged.

References

[1] Thorsen, T., Roberts, R. W., Arnold, F. H. and Quake, S. R. 2001, 'Dynamic pattern formation in a vesicle-generating microfluidic device' *Phys. Rev. Lett.* 86, 4163

[2] Dreyfus, R., Tabeling, P., and Willaime, H. 2003, 'Ordered and disordered patterns in two -phase flow in microchannels' *Phys. Rev. Lett.* 90, 144505

[3] Song, H., Chen, D. L., and Ismagilov, R. F. 2006, 'Droplets in microfluidic channels' *Angew. Chem. Int. Ed.* 45, 7336-7356

[4] Teh, S. Y., Lin, R., Hung, L. H., and Lee, A.P.2008, 'Droplets microfluidics' *Lab-on-chip* 8, 198-220

[5] Baroud, C. N., and Willaime, H. 2004, 'Multiphase flows in microfluidics' *C. R. Physique*. 5, 547-555

[6] Sahimi, M. 1993, 'Flow phenomena in rocks: from continum models to fractals, percolation, cellular automata and simulated annealing' *Rev. Mod. Phys* 65, 1393

[7] Grotberg, J. B. and Jensen, O. E. 2004, 'Biofluid mechanics of flexible tubes.' *Annu. Rev. Fluid Mech* 36, 121

[8] Halpern, D., Fujioka, H., Takayama, S. and Grotberg, J. B. 2008. 'Liquid and surfactant delivery into the pulmonary airways' *Respir Neurobiol* 163

[9] Hazel, A. E. and Heil, M. 2002, 'The steady propagation of a semi-infinite bubble into a tube of elliptical or rectangular cross-section' *J. Fluid Mechanics* 470, 91-114

[10] Clanet, C., Herault, P. and Searby, G. 2004, 'On the motion of bubbles in vertical tubes of arbitrary Cross-sections: some complements to the Dumitrescu-Taylor problem.' *J. Fluid Mechanics* 519, 359-376

[11] Taylor, G. I. 1961 'Deposition of viscous fluid on the wall of a tube.' *J. Fluid Mechanics* 10, 161-165

[12] Whitesides, G. M. 2006, 'The origins and future of microfluidics' *Nature* 442, 368

[13] Hollis, C., Vahrenkamp, V., Tull, S., Mookerjee, A., Taberner, C. and Huang, Y. 2010, 'Pore system characterisation in heterogeneous carbonates: an alternative approach to widely used rock-typing methodologies. *Marine and Petroleum Geology* 27, 772-793

[14] Heap, A. and Juel, A. (2008), 'Anomalous bubble propagation in elastic tubes', *Physics of fluids* 20, 081702

[15] Pailha, M., Hazel, A. L., Glendinning, P. A. and Juel, A. 2012, 'Oscillatory bubbles induced by geometrical constraint.' *Phy. of Fluids* 24, 021702

[16] De Lozar, A., Heap, A., Hazel, A. L., and Juel, A.(2009). 'Tube geometry can force switchlike transition in the behaviour of propagating bubbles' *Physics of Fluids* 21, 101702

[17] Hazel, A. L., Pailha, M, Cox, S. J., and Juel, A. (2013),'Multiple states of finger propagation in partially occluded tubes' *Physics of Fluids* 25, 062106

[18] Thompson, A. B., Juel, A. and Hazel, A. L. (2013), 'Multiple finger propagation modes in Hele-Shaw cells of variable depth.', *Journal of fluid Mechanics* (under review).

[19] De Lozar, A., Juel, A., and Hazel, A. L.(2008), 'The steady of propagation of an air finger into a rectangular tube', *Journal of fluid Mechanics* 614, 173-195

[20] Baroud, C. N., Gallaire, F. and Dangla, R. (2010). 'Dynamics of microfluidic droplet', *Journal of the royal society of chemistry*. 10, 2032-2045.

[21] Fuerstman, M. J., Garstecki, P. and Whitesides, G. M. (2007) 'Coding/Decoding and Reversibility of Droplets trains in microfluidic networks', *Science*. 315, 828.

[22] Prakash, M. and Gershenfeld, N. (2007), 'Microfluidic bubble logic', *Science*. 315, 832.

[23] Juel, A. and Alexandra, H.(2007), 'The reopening of a collapsed fluid-filled elas- tic tube', *Journal of fluid Mechanics* 572, 287-310

[24] Saffman, P. G. and Taylor, G. I. (1958). 'The penetration of a fluid into a porous medium or Hele-Shaw cell containing a more viscous liquid', *Proc. R. Soc. Lond* . 245, 312-329

[25] Hooman, F., and Masahiro, K. 2011, 'Viscous oil-water flows in a microchannel initially saturated with oil: Flow patterns and pressure drop characteristics' *Int. J. of Multiphase Flow* 37, 1147-1155

[26] Lichao, P., 2013, 'Complex fluids in microchannel flows at low Reynolds number: Elastic instabilities and rheology' *Ph.D Dissertation.*

[27] Mbanjwa, M.B., Land, K. J., Jewell, L., Moss, E. A. and Gledhill, I. M. A. 2010, 'Experimental observation of capillary instabilities of two phase flow in microfluidic T-Junction' *SACAM.* 7, 1-9

[28] Jisiou, M., Dawson, G., Thompson, A. B., Mohr, S., Feilden, P. R., Hazel, A. L., and Juel, A. 2014, 'Geometry-induced oscillations of finite bubbles in microchannels' *Procedia IUTAM* 11, 81-88:

Zuonaki Ongodiebi / Adokiye Omoghoyan
Department of Mathematics and Computer Science, Niger Delta University, Bayelsa State, Nigeria.
Email: zuonaki_bribai@yahoo.com